Hydrol. Earth Syst. Sci. Discuss., 11, 11883–11904, 2014
www.hydrol-earth-syst-sci-discuss.net/11/11883/2014/
doi:10.5194/hessd-11-11883-2014

Hydrology and Earth System Sciences
Open Access
Discussions

Technical Note: Surface water velocity observations from a camera: a case study on the Tiber River

F. Tauro[1], G. Olivieri[1], A. Petroselli[2], M. Porfiri[3], and S. Grimaldi[1]

[1]Dipartimento per l'innovazione nei sistemi biologici, agroalimentari e forestali, University of Tuscia, Viterbo, Italy
[2]Dipartimento di scienze e tecnologie per l'agricoltura, le foreste, la natura e l'energia, University of Tuscia, Viterbo, Italy
[3]Department of Mechanical and Aerospace Engineering, New York University Polytechnic School of Engineering, Brooklyn, NY USA

Received: 5 September 2014 – Accepted: 9 October 2014 – Published: 24 October 2014

Correspondence to: S. Grimaldi (salvatore.grimaldi@unitus.it)

Published by Copernicus Publications on behalf of the European Geosciences Union.

Abstract

Monitoring surface water velocity during flood events is a challenging task. Techniques based on deploying instruments in the flow are often unfeasible due to high velocity and abundant sediment transport. A low-cost and versatile technology that provides continuous and automatic observations is still not available. LSPIV (large scale particle imaging velocimetry) is a promising approach to tackle these issues. Such technique consists of developing surface water velocity maps analyzing video frame sequences recorded with a camera. In this technical brief, we implement a novel LSPIV experimental apparatus to observe a flood event in the Tiber river at a cross-section located in the center of Rome, Italy. We illustrate results from three tests performed during the hydrograph flood peak and recession limb for different illumination and weather conditions. The obtained surface velocity maps are compared to the rating curve velocity and to benchmark velocity values. Experimental findings confirm the potential of the proposed LSPIV implementation in aiding research in natural flow monitoring.

1 Introduction

Stream flow is pivotal for a variety of hydro-environmental studies. Namely, cross-section velocity is functional for several hydrological analyses, including rainfall–runoff (Grimaldi et al., 2010), hydraulic propagation (Kreibich et al., 2009), erosion models (Zeng et al., 2008), and rating curves (McMillan et al., 2010). Standard techniques for measuring stream water velocity vary with the dimension of the channel, its accessibility, and its hydraulic regime. Flow-meters, chemical tracers, and dyes are still the most common methods in the analysis of large river cross-sections, as well as small impervious channels (Buchanan and Somers, 1969; Planchon et al., 2005; Leibundgut et al., 2009; Tazioli, 2011; Hrachowitz et al., 2013; deLima and Abrantes, 2014). Alternative methodologies are based on acoustic Doppler instrumentation (ADI) (Yorke and Oberg, 2002) or remote sensing observations, that is, hand-held radar, microwave

HESSD
11, 11883–11904, 2014

sensors, and satellite (Fulton and Ostrowski, 2008; Alessandrini et al., 2013; Tarpanelli et al., 2013).

Most of these methods are affected by several drawbacks: they are time consuming, do not provide continuous observations, need sampling, and are intrusive. Only remote sensing approaches can afford velocity measurements without the deployment of instrumentation in the flow, thus offering continuous data acquisition. However hand-held radars and microwave sensors are relatively expensive, and satellite approaches are typically limited to large river water depths. A major implication of these limitations is that flow measurement campaigns are infrequent, so that stream velocity observations during major floods are scarce or absent.

In the last few years, large scale particle image velocimetry (LSPIV) has been proposed to overcome some of these drawbacks (Fujita et al., 1997; Bradley et al., 2002; Creutin et al., 2003; Jodeau et al., 2008; Hauet et al., 2008b, 2009; Gunawan et al., 2012; Bechle et al., 2012; Bechle and Wu, 2014). The novelty of LSPIV should be sought in its capacity of extracting desired kinematic information from a video of the surface stream flow. The basic premise of this approach is that a low-cost camera is sufficient to estimate the surface velocity of water streams. Specifically, videos of floating objects dragged by the flow are processed to estimate the velocity of the background fluid in the form of surface velocity. Open questions in LSPIV research entail establishing automatic and continuous observations in extreme hydraulic conditions.

The general implementation of LSPIV can be summarized in three main sequential steps: video recording, image pre-processing, and image analysis. The video recording is the simplest phase of LSPIV, as it can be executed with a low-cost sport camera at a standard sampling frequency (30–60 frames per second – fps) and at full-HD image resolution (1920 × 1080 pixels). The best configuration depends on the geometric characteristics of the stream cross-section, and several high performance and versatile low-cost cameras (up to 240 fps and up to 4K – 4096 × 2160 pixels resolution) are currently available. Image pre-processing is necessary for treating video frames before the image analysis. Typical pre-processing includes pixel calibration, frame correction,

HESSD
11, 11883–11904, 2014

and frame matching, to compensate for distortions and undesired mechanical vibrations. In this context, we have recently proposed a novel apparatus to enable LSPIV of water streams (Tauro et al., 2014), which utilizes low-cost cameras and lasers to enable the acquisition of high throughput data and improve experimental efficiency. The treated frame sequence is ultimately processed through standard PIV algorithms that return the sought velocity maps. PIV (Adrian, 1991; Raffel et al., 2007) is based on the cross-correlation of pairs of consecutive frames, in which each frame is subdivided into interrogation windows that are translated on a pixel grid.

LSPIV accuracy is affected by the presence of floating objects in the stream (Muste et al., 2008; Kim, 2006). While non-stationary ripples present in the water flow are sometimes sufficient for the analysis (Creutin et al., 2003; LeCoz et al., 2010), LSPIV is often benefited by natural or artificial tracer seeding, which aids in the velocity reconstruction (Dramais et al., 2011; Tauro et al., 2012, 2013a, b). The abundance of natural material is expected to suffice for the study of flood events.

In this technical brief, a sample application of LSPIV is proposed to study a flood. Specifically, the experimental apparatus recently proposed in (Tauro et al., 2014) is utilized to study a flood event in the Tiber river in Rome, Italy. During the flood occurred in February 2014, three tests were conducted from a bridge in the center of Rome, where a historical hydrological cross-section is located. The analysis aids in understanding the potential benefit of the approach and its limitations.

The rest of this brief is organized as follows. In Sect. 2, the case study is described. The characteristics of the cross-section and the monitored flood hydrograph are also reported. Section 3 summarizes the experimental apparatus proposed in (Tauro et al., 2014), highlighting the roles of external lasers in the image calibration. Therein, we also detail the image analysis, addressing both methodological issues and practical aspects. In Sect. 4, we summarize our findings and comments on future improvements of the methodology, specifically concerning the interpretation of the velocity maps.

HESSD
11, 11883–11904, 2014

2 Case study site and experiment description

Three experiments were performed at the Ripetta cross-section located in the center of Rome (see Fig. 1). This is an historical hydrological section, which has been monitored since the end of the 19th century by the Ufficio Idrografico e Mareografico at Regione Lazio (UIMRL). The UIMRL regularly updates the rating curve with standard and advanced direct discharge measurements, and records water levels every 15 min through an ultrasonic water meter installed at the bridge mid-span.

The flood event occurred in the first two weeks of February 2014. The peak discharge, estimated to be equal to 1621 $m^3 s^{-1}$ from the rating curve, corresponds to a 10 year return period. Figure 2 shows the hydrograph shape with water levels and discharge values. Therein, the three tests are indicated to pinpoint the flow regime during the experiments along with the bridge level to quantify the distance between the camera and the water surface.

The first test (Test1) was conducted during the main hydrograph peak, the second one (Test2) at the beginning of the first recession limb, and the last one (Test3) during the second flood peak. The three tests were performed at different times of the day (evening, middle of the day, and afternoon, respectively) to evaluate the effect of different illumination conditions on LSPIV. Importantly, during the flood, considerable amount of natural floating materials was present in the flow (Fig. 1c).

The apparatus was installed on the parapet at the bridge mid-span (Fig. 1b). The field of view (FOV) included the central portion of the entire cross-section to estimate the maximum surface velocity of the river. The averaged cross-section flow velocities and discharge from UIMRL rating curve are reported in Fig. 2; these values represent an average on both surface and cross-areal velocities. To offer a further means of comparison for LSPIV, we also measured the flow velocity by manually quantifying the number of frames that a clearly visible object needed to transit in the FOV. These benchmark values are expected to be close to the maximum flow velocity, since they pertained to objects floating in the middle of the surface section (Fig. 1c).

HESSD
11, 11883–11904, 2014

3 Experimental apparatus and image analysis procedure

The proposed platform includes a low-cost camera (GoPro Hero 3) installed on a telescopic hollow aluminum bar to maintain its axis orthogonal to the water surface (Fig. 3a). Its main novelty with respect to current LSPIV implementations is the use of two lasers that are installed at the ends of a 1 m pole connected to the bar. Such lasers create reference points in the FOV that are crucial for pixel calibration (Fig. 3b), which would instead require surveying through GPS or total stations (Hauet et al., 2008a; Kantoush et al., 2011). By dispensing with the need of surveying reference fixed points, the platform versatility is increased, allowing its installation under river bridges, on hydrological cable-ways, or aerial vehicles. In addition, the use of the telescopic bar circumvents the need for orthorectification, which is a major challenge in current LSPIV implementations (Hauet et al., 2008a).

With respect to image pre-processing, two main issues are addressed in this step: the frame distortion from the fish eye camera lens and the FOV mismatching from the camera vibrations induced by the wind. The removal of the lens distortion is addressed by simply accounting for the camera lens parameters. In fact, some sport cameras offer open source software to cope with this issue; in our experiments, we utilized the GoPro studio software (http://shop.gopro.com/softwareandapp/gopro-studio/GoPro-Studio.html) that easily removes the fish eye lens distortion, thus providing planar frames. With respect to mechanical vibrations, several approaches have been proposed in the literature (Fujita and Hino, 2013; Fujita and Kunita, 2011). Based on results in (Tauro et al., 2014), we opted for a FOV matching approach, which is based on the cross-correlation between captured images and a template sub-image that depicts an object visible in all frames. Matched images are trimmed by fixed pixel lengths around the template position to depict overlapping FOVs.

The consecutive sequence of undistorted and FOV-matched calibrated frames is finally fed into the PIV algorithm (Gui, 2013) to extract the FOV velocity map. The algorithm entails the transformation of the frame in a raster grid of interrogation windows.

HESSD
11, 11883–11904, 2014

Each interrogation window is cross-correlated with a larger search window in the next frame. Typically, a larger search window is defined by shifting the interrogation window by half its dimension in every direction. The maximum cross-correlation value indicates the cell displacement that directly relates to the sought velocity. The algorithm is iterated for each cell in the frame and for each pair of consecutive frames. Following this procedure, surface flow velocity maps are constructed for each pair of consecutive images. Time-averaged maps are then obtained by averaging selected sequences of images.

Thus, three parameters should be assigned for the algorithm execution: video resolution, video frequency, and grid cell dimension or interrogation window (in pixel). Here, we used the parameter set proposed in (Tauro et al., 2014), namely, VGA resolution (640 × 480 pixels), 30fps frequency, and 32 × 32 pixels interrogation window.

4 Results and discussion

Three tests were conducted during the flood event in February 2014. Test1 monitored the flow in the proximity of the maximum flood discharge in the evening, under heavy rain; Test2 monitored the flow during the recession limb in the middle of a sunny day with scattered clouds; and Test3 monitored the second flood peak in the afternoon of a cloudy day. Videos were recorded at full-HD resolution and 60fps for two minutes of duration each, and they were subsequently reduced to VGA resolution and resampled to 30fps, so that the resulting 3600 consecutive frames were spaced in time by 0.033 s. The FOV dimensions were 32 m × 16 m (Test1), 32 m × 17 m (Test2), and 46 m × 24 m (Test3), corresponding to approximately 30 % of the entire river cross-section surface. Notably, FOV dimensions for Test3 differ from the other trials due to the larger distance between the camera and the water, as shown in Fig. 2. The LSPIV algorithm was applied on a sequence of 500 frames, which was extracted to guarantee a sufficient transit of floating material.

HESSD
11, 11883–11904, 2014

Figure 4 displays a few snapshots of the 500 frames considered in Test2, which was executed in the most favorable weather and illumination conditions. The first row depicts VGA frames subsampled at 30 Hz, while the second and third rows display the modified frames after compensating for the lens distortion and performing the FOV matching, respectively. We comment that image treatment required to address distortions and vibrations is minimal as compared to orthorectification that is commonly required in LSPIV with angled cameras. In Fig. 4, different hydraulic behaviors are visible. Specifically, near the bridge pier (bottom left) a section reduction effect with local increase of water velocity is evident; in the upper part (top left), there is an opposite effect with a lower velocity zone; and in the remaining FOV, the presence of homogeneous ripples indicate the presence of main stream flow.

Figure 5 illustrates the FOV velocity maps obtained from the three tests. Velocity values of each node represent the average of velocity values estimated on the available 499 pairs of consecutive frames. The most satisfactory results are those in the middle panel of Fig. 5, where homogenous velocity vectors are obtained and the kinematics around and before the bridge pier is well reproduced. This should be attributed to the favorable illumination and weather conditions of Test2 and to the fact that the FOV was well centered within the river. The least satisfactory velocity map is instead the one corresponding to Test1 and reported in the top panel of Fig. 5. Test1 was in fact performed in the evening and during rainfall. Notably, velocities estimated in Test1 pertain to few artificially illuminated areas on the water surface in the proximity of the bridge.

Our results suggest that time averaged velocity maps tend to underestimate the surface flow velocity. In fact, the river surface velocity corresponds to local data only in the ideal case of a fully homogeneous transit of floating material and perfect illumination conditions. This is also evident from Fig. 5, where a considerable variability of the velocity is noted, with several nodes yielding a null velocity. Such false readings are due to the absence of visible tracers in the frame sequence, rather than to placid water. To offer further insight on the temporal and spatial variability of the estimated velocity field, three cross-section profiles (at 2, 8, and 15 m from the bottom of the FOV) are shown

HESSD
11, 11883–11904, 2014

in Fig. 6. Therein, the colored interval represents the standard deviation (SD) over the values estimated on the 499 frame pairs. The large variation of the flow velocity is an additional indication of the role of the illumination and the floating material, which both contribute to false readings along the water flow.

If the aim of the monitoring experiment is the determination of a velocity value for rating curve calibration, homogeneous sub-FOVs should be selected, excluding either fixed objects in images or FOV sectors that are not indicative of the main stream flow. For the three tests, suitable sub-FOVs are displayed in Fig. 7; their dimensions are 6 m × 14 m (Test1), 7 m × 13 m (Test2), and 10 m × 15 m (Test3).

Even if the sub-FOVs represent more homogeneous scenarios for PIV analysis, representative velocity values should not be estimated as spatial averages in such regions, due to the ubiquitous presence of false readings from irregular transit of floating material. To clarify this aspect, in Table 1, we report sub-FOV average velocities along with the 80, 85, 90, 95, and 99 percentiles and the coefficient of variation of the sub-FOV velocity value distribution. For completeness, these values are compared to the rating curve values and manually supervised benchmark data. As expected, the average velocity is significantly smaller than the benchmark values, while the 99 percentile seems to well describe the flow velocity. The low coefficients of variations in Test1 and Test2 are particularly encouraging, even if the adverse weather and illumination conditions certainly affect the accuracy of the results.

5 Conclusions

In this technical brief, a sample implementation of LSPIV for surface water velocity measurements during a flood event is described. The technique is capable of quantifying the surface flow without the need of deploying instrumentation but only analyzing video frames of the river flow. The approach has the potential to yield automatic, continuous, and low-cost observations in adverse conditions, which more conventional techniques cannot guarantee. In the considered case study, the feasibility of a novel experimental

HESSD
11, 11883–11904, 2014

apparatus is tested by monitoring a flood event in the Tiber river at a cross-section located in the center of Rome, Italy. The main novelty of the proposed platform consists of the use of lasers for calibrating the frame pixel dimensions, thereby enhancing the versatility of the technique. In addition, the platform minimizes the need for image orthorectification by using a telescopic bar to maintain the camera orthogonal to the river flow.

Three tests were executed during a 10 year return period flood event in different illumination and weather conditions. A sequence of 500 frames at VGA resolution and 30fps frequency was input to the LSPIV algorithm. The obtained velocity maps were compared to values related to the cross-section rating curves, as well as to manual observations garnered from the analysis of the videos. Consistent with the literature, the obtained velocity map displays high spatial variability due to the intermittent and spatially heterogeneous transit of floating material. However, analysis of the acquired videos indicates that the effects of such variability can be mitigated by focusing on smaller fields of view and considering velocity distributions, rather than average values.

Our findings suggest that future research should focus on devising a calibration procedure for identifying representative velocity values through salient indices of temporal and spatial variations. Furthermore, extensive analyses are necessary to establish criteria for selecting the duration of image sequences. Previous studies (Kim, 2006) have proposed that longer sequences would provide less heterogeneous velocity maps, however this choice should be related to the amount and the distribution of floating materials present during the monitored flood event. In general, our analysis confirms that LSPIV is a promising technique to aid in river flow monitoring in challenging conditions.

The Supplement related to this article is available online at doi:10.5194/hessd-11-11883-2014-supplement.

HESSD
11, 11883–11904, 2014

Acknowledgements. This work was supported by the American Geophysical Union Horton (Hydrology) Research Grant for Ph.D. students, by the Ministero degli Affari Esteri e Cooperazione Internazionale project 2014 Italy-USA PGR00175, by the Honors Center of Italian Universities, and by the National Science Foundation under grant number BCS-1124795. The authors thank Roberto Rapiti and Giuliano Cipollari for help with the experiments and Francesco Mele, Domenico Spina, and Luigi D'Aquino from UIM for providing water level measurements and rating curves.

References

Adrian, R. J.: Particle-imaging techniques for experimental fluid-mechanics, Annu. Rev. Fluid Mech., 23, 261–304, 1991.

Alessandrini, V., Bernardi, G., and Todini, E.: An operational approach to real-time dynamic measurement of discharge, Hydrol. Res., 44, 953–964, 2013.

Bechle, A., Wu, C., Liu, W., and Kimura, N.: Development and application of an automated river-estuary discharge imaging system, J. Hydraul. Eng., 138, 327–339, 2012.

Bechle, A. J. and Wu, C. H.: An entropy-based surface velocity method for estuarine discharge measurement, Water Resour. Res., 50, 6106–6128, 2014.

Bradley, A. A., Kruger, A., Meselhe, E. A., and Muste, M. V. I.: Flow measurement in streams using video imagery, Water Resour. Res., 38, 1–8, 2002.

Buchanan, T. J. and Somers, W. P.: Discharge measurements at gaging stations: US Geological Survey techniques of water-resources investigations, Tech. rep., US Geological Survey,Arlington, VA, 1969.

Creutin, J. D., Muste, M., Bradley, A. A., Kim, S. C., and Kruger, A.: River gauging using PIV techniques: a proof of concept experiment on the Iowa River, J. Hydrol., 277, 182–194, 2003.

deLima, J. L. M. P. and Abrantes, J. R. C. B.: Using a thermal tracer to estimate overland and rill flow velocities, Earth Surf. Proc. Land., 39, 1293–1300, 2014.

Dramais, G., LeCoz, J., Camenen, B., and Hauet, A.: Advantages of a mobile LSPIV method for measuring flood discharges and improving stage-discharge curves, J. Hydro-Environ. Res., 5, 301–312, 2011.

Fulton, J. and Ostrowski, J.: Measuring real-time streamflow using emerging technologies: radar, hydroacoustics, and the probability concept, J. Hydrol., 357, 1–10, 2008.

HESSD

11, 11883–11904, 2014

Fujita, I. and Hino, T.: Unseeded and seeded PIV measurements of river flows video from a helicopter, J. Visual.-Japan, 6, 245–252, 2003.
Fujita, I. and Kunita, Y.: Application of aerial LSPIV to the 2002 flood of the Yodo River using a helicopter mounted high density video camera, J. Hydroenviron. Res., 5, 323–331, 2011.
Fujita, I., Muste, M., and Kruger, A.: Large-scale particle image velocimetry for flow analysis in hydraulic engineering applications, J. Hydraul. Res., 36, 397–414, 1997.
Grimaldi, S., Petroselli, A., Alonso, G., and Nardi, F.: Flow Time estimation with variable hillslope velocity in ungauged basins, Adv. Water Resour., 33, 1216–1223, 2010.
Gui, L.: EDPIV – Evaluation Software for Digital Particle Image Velocimetry, available at: http://lcgui.net, 2013.
Gunawan, B., Sun, X., Sterling, M., Shiono, K., Tsubaki, R., Rameshwaran, P., Knight, D., Chandler, J., Tang, X., and Fujita, I.: The application of LS-PIV to a small irregular river for inbank and overbank flows, Flow Meas. Instrum., 24, 1–12, 2012.
Hauet, A., Creutin, J. D., and Belleudy, P.: Sensitivity study of large-scale particle image velocimetry measurement of river discharge using numerical simulation, J. Hydrol., 349, 178–190, 2008a.
Hauet, A., Kruger, A., Krajewski, W. F., Bradley, A., Muste, M., Creutin, J.-D., and Wilson, M.: Experimental system for real-time discharge estimation using an image-based method, J. Hydrol. Eng., 13, 105–110, 2008b.
Hauet, A., Muste, M., and Ho, H.-C.: Digital mapping of riverine waterway hydrodynamic and geomorphic features, Earth Surf. Proc. Land., 34, 242–252, 2009.
Hrachowitz, M., Savenije, H., Bogaard, T. A., Tetzlaff, D., and Soulsby, C.: What can flux tracking teach us about water age distribution patterns and their temporal dynamics?, Hydrol. Earth Syst. Sci., 17, 533–564, doi:10.5194/hess-17-533-2013, 2013.
Jodeau, M., Hauet, A., Paquier, A., Le Coz, J., and Dramais, G.: Application and evaluation of LS-PIV technique for the monitoring of river surface velocities in high flow conditions, Flow Meas. Instrum., 19, 117–127, 2008.
Kantoush, S. A., Schleiss, A. J., Sumi, T., and Murasaki, M.: LSPIV implementation for environmental flow in various laboratory and field cases, J. Hydroenviron. Res., 5, 263–276, 2011.
Kim, Y.: Uncertainty analysis for non-intrusive measurement of river discharge using image velocimetry, Ph.D. thesis, Graduate College of the University of Iowa, 2006.

HESSD
11, 11883–11904, 2014

Kreibich, H., Piroth, K., Seifert, I., Maiwald, H., Kunert, U., Schwarz, J., Merz, B., and Thieken, A. H.: Is flow velocity a significant parameter in flood damage modelling?, Nat. Hazards Earth Syst. Sci., 9, 1679–1692, doi:10.5194/nhess-9-1679-2009, 2009.

LeCoz, J., Hauet, A., Pierrefeu, G., Dramais, G., and Camenen, B.: Performance of image-based velocimetry LSPIV applied to flash-flood discharge measurements in mediterranean rivers, J. Hydrol., 394, 42–52, 2010.

Leibundgut, C., Maloszewski, P., and Külls, C.: Tracers in hydrology, Wiley-Blackwell, Oxford, 2009.

McMillan, H., Freer, J., Pappenberger, F., Krueger, T., and Clark, M.: Impacts of uncertain river flow data on rainfall–runoff model calibration and discharge predictions, Hydrol. Process., 24, 1270–1284, 2010.

Muste, M., Fujita, I., and Hauet, A.: Large-scale particle image velocimetry for measurements in riverine environments, Water Resour. Res., 44, W00D19, doi:10.1029/2008WR006950, 2008.

Planchon, O., Silvera, N., Gimenez, R., Favis-Mortlock, D., Wainwright, J., Le Bissonnais, Y., and Govers, G.: An automated salt-tracing gauge for flow-velocity measurement, Earth Surf. Proc. Land., 30, 833–844, 2005.

Raffel, M., Willert, C. E., Wereley, S. T., and Kompenhans, J.: Particle Image Velocimetry. A practical guide, Springer, New York, 2007.

Tarpanelli, A., Barbetta, S., Brocca, L., and Moramarco, T.: River discharge estimation by using altimetry data and simplified flood routing modeling, Remote Sens., 5, 4145–4162, 2013.

Tauro, F., Grimaldi, S., Petroselli, A., and Porfiri, M.: Fluorescent particle tracers in surface hydrology: a proof of concept in a natural stream, Water Resour. Res., 48, W06528, doi:10.1029/2011WR011610, 2012.

Tauro, F., Porfiri, M., and Grimaldi, S.: Fluorescent eco-particles for surface flow physics analysis, AIP Advances, 3, 032108, doi:10.1063/1.4794797, 2013a.

Tauro, F., Rapiti, E., Al-Sharab, J. F., Ubertini, L., Grimaldi, P., and Porfiri, M.: Characterization of eco-friendly fluorescent nanoparticle doped-tracers for environmental sensing, J. Nanopart. Res., 15, 1884, doi:10.1007/s11051-013-1884-y, 2013b.

Tauro, F., Porfiri, M., and Grimaldi, S.: Orienting the camera and firing lasers to enhance large scale particle image velocimetry for stream flow monitoring, Water Resour. Res., 50, 7470–7483, doi:10.1002/2014WR015952, 2014.

HESSD
11, 11883–11904, 2014

Tazioli, A.: Experimental methods for river discharge measurements: comparison among tracers and current meter [Méthodes expérimentales pour mesurer le débit des cours d'eau: comparaison entre les traceurs artificiels et le courantomètre], Hydrolog. Sci. J., 56, 1314–1324, 2011.

Yorke, T. H. and Oberg, K. A.: Measuring river velocity and discharge with acoustic Doppler profilers, Flow Meas. Instrum., 13, 191–195, 2002.

Zeng, J., Constantinescu, G., Blanckaert, K., and Weber, L.: Flow and bathymetry in sharp open-channel bends: experiments and predictions, Water Resour. Res., 44, W09401, doi:10.1029/2007WR006303, 2008.

HESSD
11, 11883–11904, 2014

Table 1. Velocities obtained for the sub-FOV of each analyzed tests. The symbol v_m refers to the velocity obtained by averaging over the selected frame sequence and the captured sub-FOV; β_v is defined as the ratio of the standard deviation (SD) of the velocity over the entire sub-FOV to v_m; v_{80}, v_{85}, v_{90}, v_{95}, and v_{99} indicate the 80, 85, 90, 95, and 99 percentiles, respectively; v_{rt} refers to the velocity estimated from the rating curve; and v_s indicates the velocity obtained from supervised visual inspection of the frames.

Test	v_m ($m\,s^{-1}$)	β_v ($m\,s^{-1}$)	v_{80} ($m\,s^{-1}$)	v_{85} ($m\,s^{-1}$)	v_{90} ($m\,s^{-1}$)	v_{95} ($m\,s^{-1}$)	v_{99} ($m\,s^{-1}$)	v_{rt} ($m\,s^{-1}$)	v_s ($m\,s^{-1}$)
1	1.32	0.75	2.07	2.48	2.77	3.48	3.92	1.36	5.02
2	2.38	0.13	2.66	2.74	2.79	2.86	3.01	1.20	3.28
3	3.09	0.19	3.58	3.65	3.75	3.87	4.12	1.09	4.54

HESSD
11, 11883–11904, 2014

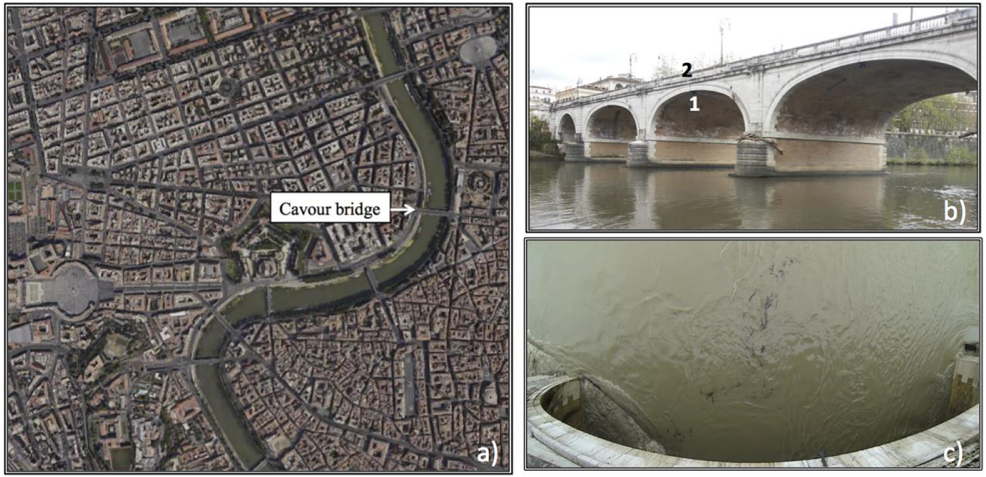

Figure 1. Ripetta cross-section, located in center of Rome under the Cavour bridge. **(a)** Map of the Tiber river in the Rome urban area, displaying the location of the Cavour bridge. **(b)** View of the Cavour bridge; the UIMRL ultrasonic water meter and the experimental apparatus are located in "1" and "2", respectively. **(c)** A picture of the floating material present during the tests.

HESSD
11, 11883–11904, 2014

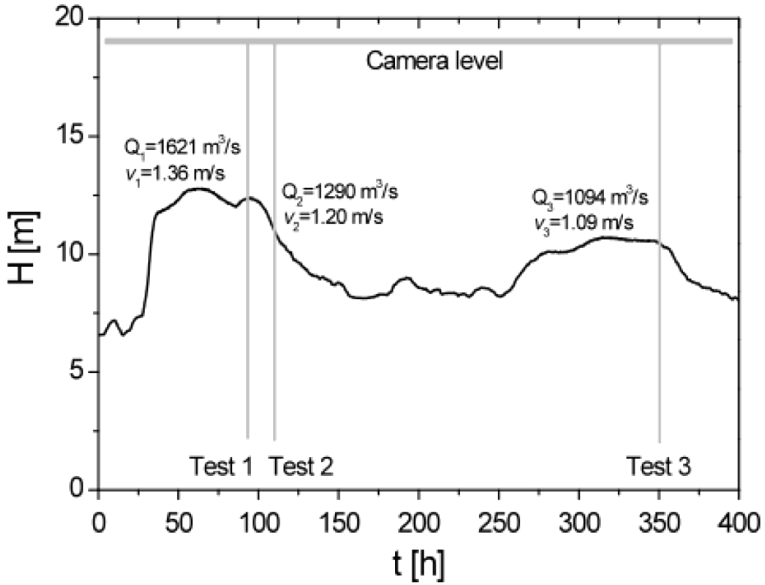

Figure 2. Hydrograph of the monitored flood event. The three tests and the related discharge and velocity values estimated by the rating curves are also displayed. The camera level corresponds to the bridge parapet height.

HESSD
11, 11883–11904, 2014

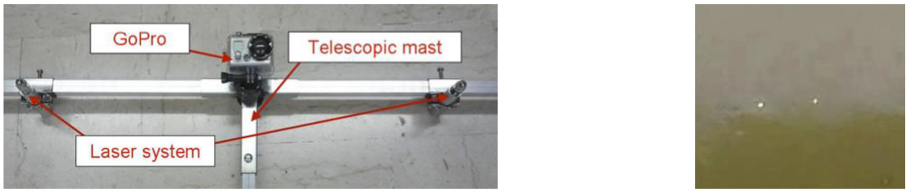

a)

b)

Figure 3. (a) View of the experimental apparatus and **(b)** lasers' trace on the Tiber river.

HESSD
11, 11883–11904, 2014

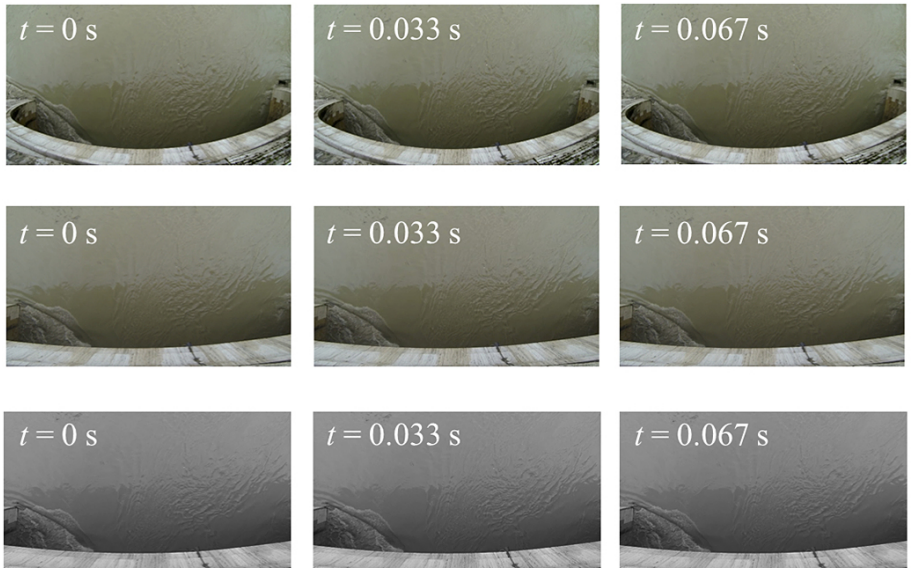

Figure 4. Snapshots depicting the FOV captured during Test2. From top to bottom, pictures are corrected for lens distortion and processed through the FOV matching procedure.

HESSD
11, 11883–11904, 2014

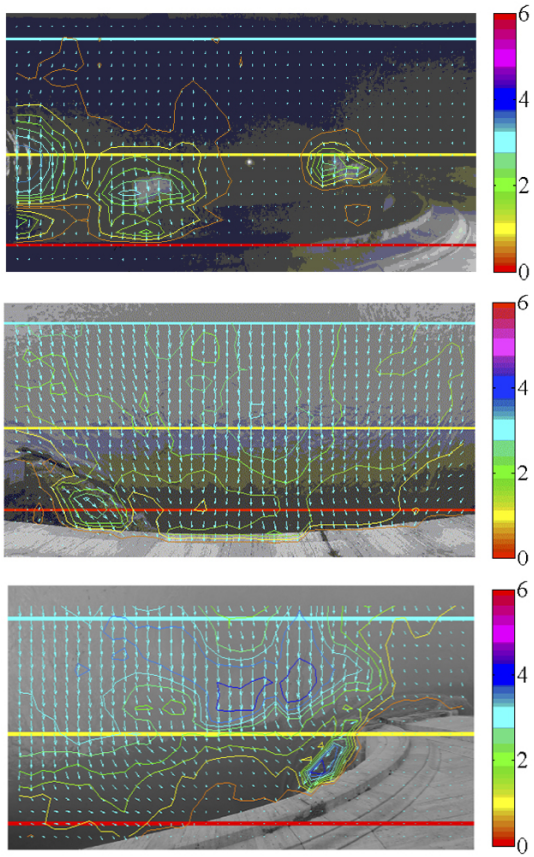

Figure 5. Time averaged surface flow velocity maps for the three tests (1, 2, and 3 from top to bottom). Values are in m s^{-1}. Solid red, yellow, and cyan lines indicate cross-sections at 2, 8, and 15 m from the bottom of the FOV, respectively.

HESSD
11, 11883–11904, 2014

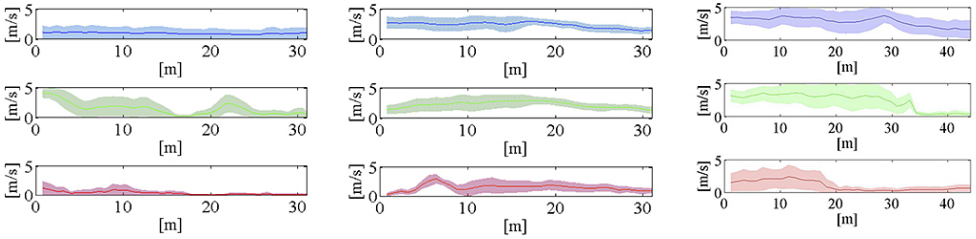

Figure 6. From top to bottom, time averaged surface flow velocity profiles for the river cross-sections at 15, 8, and 2 m from the bridge obtained from the three experiments. Shaded areas indicate the SD over the 499 pairs of frames. From left to right, Test1, Test2, and Test3 are reported, respectively.

HESSD
11, 11883–11904, 2014

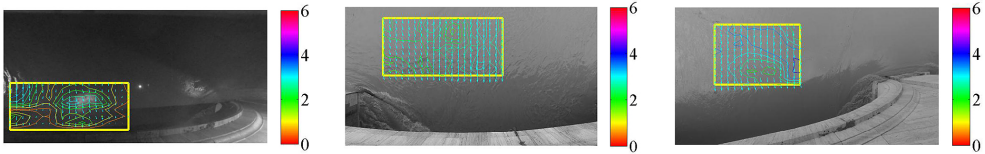

Figure 7. Sub-FOVs for unique velocity value estimation. From left to right, Test1, Test2, and Test3 are reported, respectively.

HESSD
11, 11883–11904, 2014